

SCIENTIFIC REPORTS

OPEN

Ti₁₂C₆₈: A stable T_h-symmetry hollow cage

Ling-Yan Ai^{1,2}, Hui-Yan Zhao¹, Hong-Man Ma¹, Jing Wang¹ & Ying Liu^{1,3}

A stable T_h-symmetry Ti₁₂C₆₈ cage was systemically investigated using density functional theory. The structure of Ti₁₂C₆₈ is a hollow cage with twelve TiC₁₃ subunit of three pentagons and one hexagon. The calculated frequencies are in the range 95.1 cm⁻¹–1423.9 cm⁻¹. There are no imaginary frequencies, showing its kinetic stability. *Ab initio* molecular dynamics simulations demonstrate that the topological structure of cage-like Ti₁₂C₆₈ cluster was well maintained when the effective temperature is up to 1139 K. The natural bond orbitals analysis shows that the *d* orbit of Ti atoms form four σ bonds with the neighboring four carbon atoms in each TiC₁₃ subunit playing an important role in the cluster stability. The molecular frontier orbitals analysis indicates that Ti₁₂C₆₈ cage has a narrow HOMO-LUMO gap with metal-like property. It would be expected to enrich the species of hollow metal carbide clusters.

Recently, an exceptionally stable hollow molecule Sc₂₀C₆₀, named volleyballene¹, has been proposed. Along with suggestion for Sc₂₀C₆₀, subsequent investigations resulted in the molecules of volleyball-like shape Y and La analogues². Sc₂₀C₆₀ containing transition metals and carbon atoms belongs to the family of metal carbide clusters. Early famous metal carbide clusters, metallo-carbohedrenes (met-cars) M₈C₁₂⁺, known as a unique class of cluster materials, which have been extensively investigated^{3–5}. The ground-state structure of met-cars was once the center of debate. Early studies proposed for the containing a pentagonal dodecahedron structure similar to C₂₀, the subsequent proposal that the isomers of Ti₈C₁₂⁺ having different-symmetry structures with much lower energies^{6–16}, have been reported. In particular, the inchoative Ti₈C₁₂ geometric structure has unique bonding properties that the *d* orbitals of Ti atoms play an important role in the cluster stability. Thus, theoretical investigations focus on an explanation for the electronic structure of novel isomers systems. Results exhibit diversities due to the existence of transition metal elements^{11,14,15,17,18}. It is worth noting that the present structures of metal carbide clusters have been different with the originally established molecular model as alluded to above. Metal carbide clusters exhibit various geometric structure that determine their novel and rich physical and chemical properties^{19–28}. Geometric configuration of each type met-cars cluster plays an important role in analyzing its characteristic and exploring the absorption mechanism of small molecules^{29–31}.

Meanwhile, metal atoms^{32–36} and metal carbide cluster^{37–39} encapsulated inside different size fullerene cages form different kinds of endohedral metallofullerenes (EMF) which have attracted special attention owing to their unique structural, electronic, and magnetic properties. For example, encapsulating La atom into C₆₀ fullerene cage³⁵ was first discovered by Smalley *et al.* Later, dimetallofullerenes Ce₂@C₈₀³³, Dy₂@C₁₀₀³⁴, La₂@C₈₀³⁶, metal carbide clusterfullerenes La₂C₂@C_s(574)-C₁₀₂³⁸ and Y₂C₂@D₅(8)-C₁₀₀³⁹ have been extensively studied. It is noteworthy that endohedral metallofullerenes enrich the family of metal carbide clusters and have promising applications in different fields such as materials science⁴⁰ and medicine⁴¹. Up to now, the investigations of metal carbide clusters have become one of the highlights in nanoscience due to their exceptional stability and unique structures.

In the present work, we proposed a stable cage-like Ti₁₂C₆₈ structure and structural properties, and the stability of Ti₁₂C₆₈ cage has been systematically investigated within the density functional theory. Furthermore, the electronic properties and the natural bond orbitals analysis have been explored.

Results and Discussion

A schematic diagram of the optimized Ti₁₂C₆₈ structure is shown in Fig. 1. It is found to be a cage-like configuration with T_h symmetry, which contains twelve TiC₁₃ subunits seamed together. Each TiC₁₃ subunit, just as highlighting blue atoms constitute the unit in the left figure of Tab. 1, in which three pentagons share a single titanium atom with one hexagon. Each TiC₁₃ subunit is bound to five neighbouring TiC₁₃ subunits through C-C bonds. As seen from the Fig. 1 that the cage-like Ti₁₂C₆₈ is composed of 12 hexagons and 36 pentagonal rings

¹Department of Physics and Hebei Advanced Thin Film Laboratory, Hebei Normal University, Shijiazhuang, 050024, Hebei, China. ²North China University of Science and Technology, Tangshan, 063000, China. ³National Key Laboratory for Materials Simulation and Design, Beijing, 100083, China. Correspondence and requests for materials should be addressed to Y.L. (email: yliu@hebtu.edu.cn)

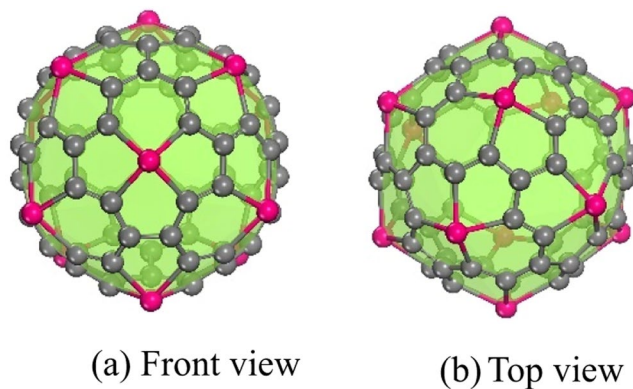


Figure 1. Front view (a) and top view (b) for cage-like $Ti_{12}C_{68}$ structure. Pink and gray spheres represent Ti and C atoms, respectively.

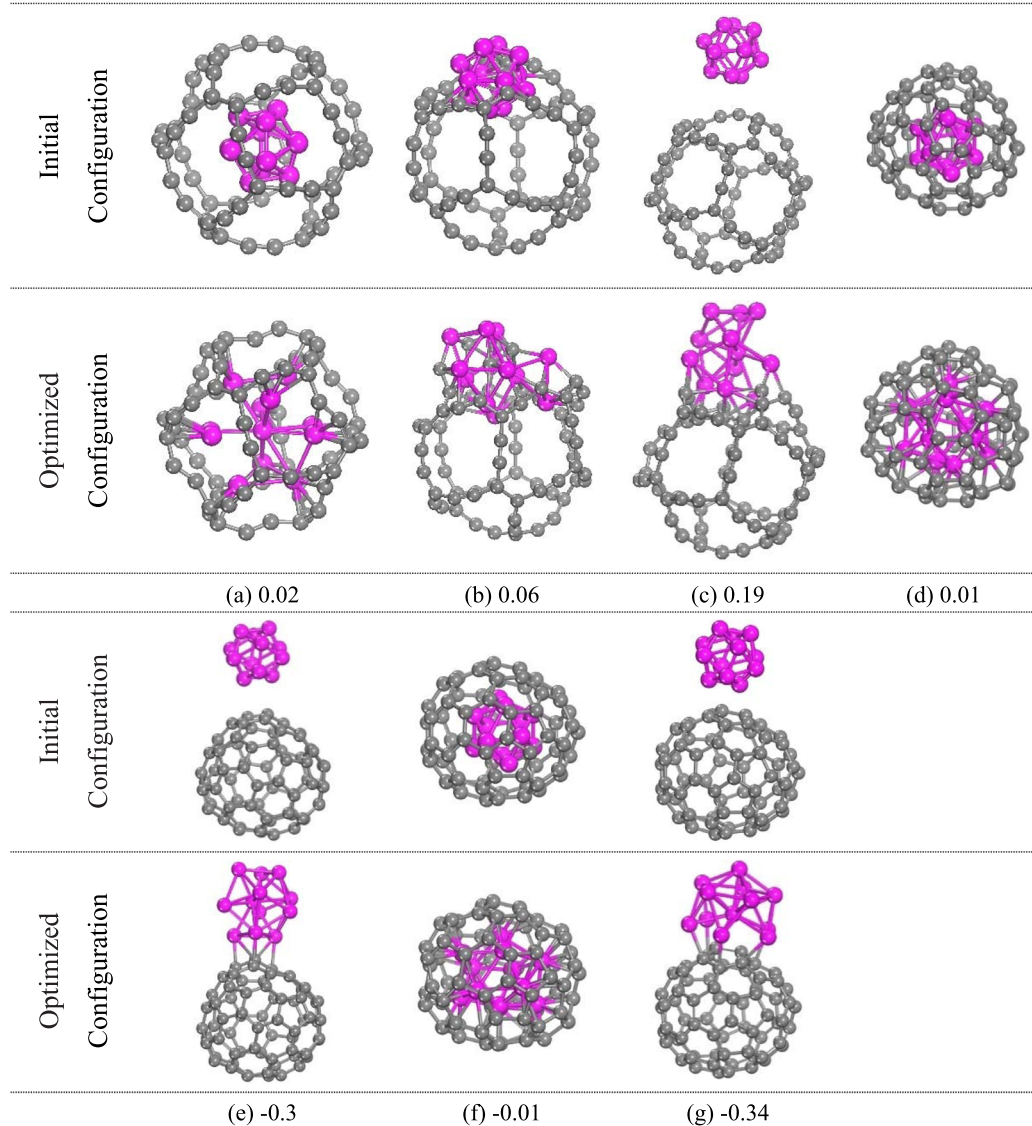


Figure 2. Three representative initial geometric structures and corresponding optimized structures of $Ti_{12}C_{68}$ cluster, which are composed by 12 titanium atoms and 68 carbon atoms, as plotted in (a–c). (d–g) Isomers of $Ti_{12}C_{68}$ cluster are composed of C_{68} fullerene and Ti_{12} . The calculated relative averaged atomic binding energies for each isomer, with respect to cage-like $Ti_{12}C_{68}$ cluster, is listed underneath each isomer. The unit of averaged binding energies is eV.

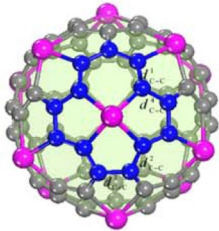
		Average bond lengths						Frequencies		E_b	E_g
		$d_{\text{Ti-C}}^1$	$d_{\text{Ti-C}}^2$	$d_{\text{C-C}}^1$	$d_{\text{C-C}}^2$	$d_{\text{C-C}}^3$	$d_{\text{C-C}}^4$	Lowest	Highest		
	PBE	2.153	2.112	1.398	1.428	1.444	1.441	95.5	1423.9	-6.86	0.05
	PW91	2.157	2.121	1.395	1.427	1.444	1.440	96.8	1410.4	-6.87	0.10
	BLYP	2.179	2.147	1.398	1.436	1.455	1.448	100.0	1360.3	-6.35	0.10

Table 1. Calculated properties for cage-like $\text{Ti}_{12}\text{C}_{68}$ structure at the GGA/PBE, GGA/PW91 and GGA/BLYP levels. The average bond lengths, the lowest and highest vibrational frequency, binding energy per atom (E_b), HOMO-LUMO gap (E_g) are listed. The units of bond lengths, frequencies, energy and charge are Å, cm^{-1} , eV and e , respectively. In the left figure, the subunit of the cage-like $\text{Ti}_{12}\text{C}_{68}$ structure is highlighted using blue atoms. Each TiC_{13} subunit is bound to five neighbouring TiC_{13} subunits through different C-C bonds. The pentagon and hexagon are connected by the two kinds different C-C bonds denoted by $d_{\text{C-C}}^1$ and $d_{\text{C-C}}^2$. The pentagons are joined by two kinds C-C bonds presented by $d_{\text{C-C}}^3$ and $d_{\text{C-C}}^4$.

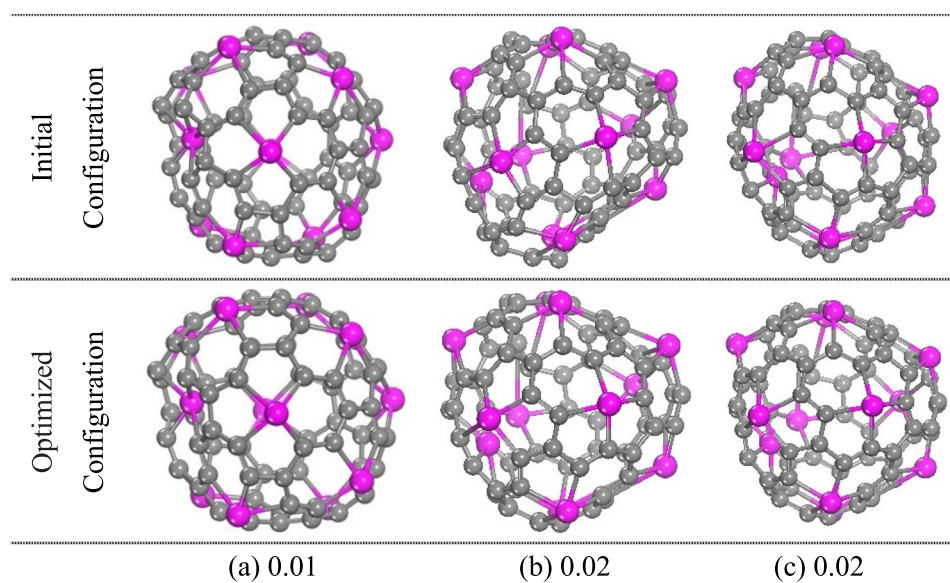


Figure 3. Initial and optimized structures for three isomers of cage-like $\text{Ti}_{12}\text{C}_{68}$ cluster. (a), (b) and (c) are three isomers which are randomly choose from the molecular dynamic simulations at initial temperature of 2000 K and 3000 K, respectively, corresponding to the effective temperature of 952 K and 1343 K. The averaged atomic binding energies in eV, relative to cage-like $\text{Ti}_{12}\text{C}_{68}$ cluster, are listed underneath each isomer.

and each of the rings contains one titanium atom. Titanium atoms occupy twelve unique positions and they have same coordination number.

In each TiC_{13} subunit, each Ti atom links four carbon atoms to form four Ti-C bonds. Ti-C bonds may be divided into two types. One type is in a hexagon denoted by $d_{\text{Ti-C}}^1$, another type is in a pentagon denoted by $d_{\text{Ti-C}}^2$. The pentagons and hexagons, and two neighbouring pentagons are connected by different C-C bonds which can be put into four categories, as shown in Table 1. As a result of bond-length equalization, such as 1, 3-butadiene, it leads C-C bond lengths lying between bond lengths of 1.54 Å (C-C bond) and 1.34 Å (C=C bond) in the optimized structure. The calculated properties of cage-like $\text{Ti}_{12}\text{C}_{68}$ are listed in Tab. 1 at the GGA/PBE, GGA/PW91 and GGA/BLYP levels, which gave the uniform structures and similar calculation results. In the following, analyses were treated within the GGA using the PBE exchange-correlation functional.

In order to search for the ground-state structure of cage-like $\text{Ti}_{12}\text{C}_{68}$ cluster, we have accomplished an extensive search with different initial configurations which are constructed with C_{68} cage and 12 Ti atoms. After relaxing these configurations, it can be found that the Ti atoms prefer to approach the carbon atoms. Three representative initial geometric structures and corresponding optimized structures are plotted in Fig. 2a-c. Note that these structures are larger in averaged atomic binding energy than the cage-like molecule by 0.02, 0.06 and 0.19 eV, respectively. In order to further compare the stability of the structure, we also construct isomers which

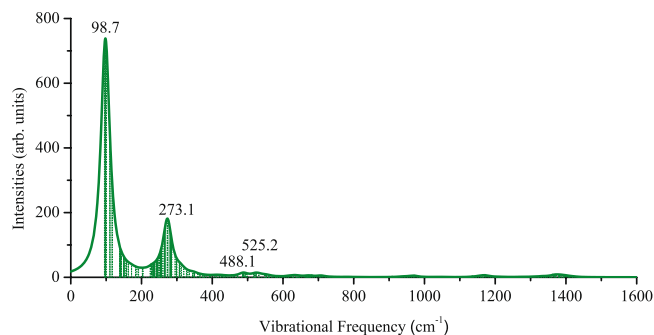


Figure 4. Raman spectrum of cage-like $\text{Ti}_{12}\text{C}_{68}$ cluster. The spectrum is broadened with a Lorentzian of 20.00 cm^{-1} .

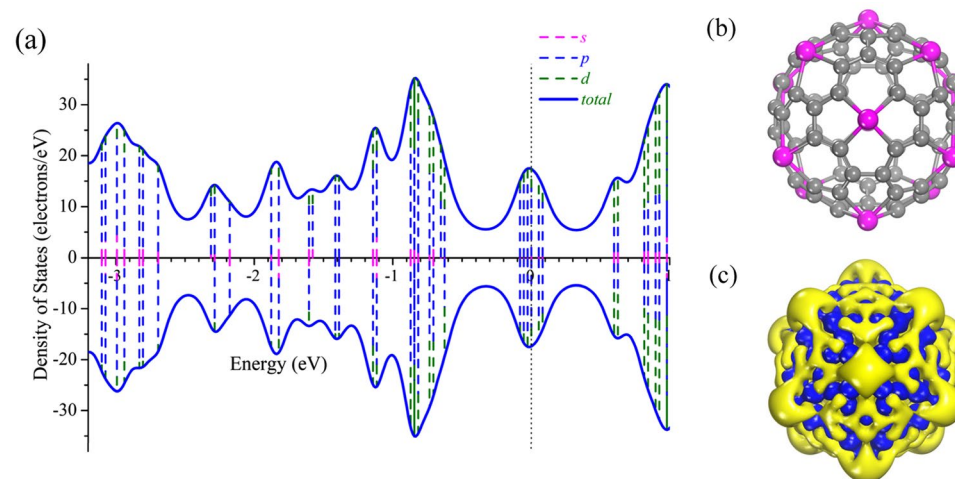


Figure 5. PDOS (a), configuration (b), and deformation electronic density (c) of cage-like $\text{Ti}_{12}\text{C}_{68}$ structure. The Fermi energy is taken as the zero energy. The isosurface for the deformation electron density corresponds to $0.03\text{ e}/\text{\AA}^3$.

are composed of C_{68} fullerene and Ti_{12} . As for C_{68} fullerene, we choose two isomers with C_1 point group plotted in (d) and (e), and C_s point group plotted in (f) and (g). The shapes of the fully optimized equilibrium structures of isomers are shown in Fig. 2(d–g). Results show that the Ti atoms prefer to be connected to the C atoms. Moreover, the isomer (d) has a 0.01 eV higher averaged atomic binding energy than the cage-like $\text{Ti}_{12}\text{C}_{68}$. (e), (f) and (g) isomers are found to be lower in averaged atomic binding energy than the cage-like molecule by 0.3, 0.01 and 0.34 eV, respectively. Thus, the cage-like $\text{Ti}_{12}\text{C}_{68}$ is a metastable structure.

In addition, in order to further confirm the stability of cage-like $\text{Ti}_{12}\text{C}_{68}$ cluster, we choose randomly three isomers with lower energy from the molecular dynamic simulations in the NVE ensemble at temperatures of 2000 and 3000 K. After energy minimization, the results revealed that the lowest-energy conformation is the cage-like $\text{Ti}_{12}\text{C}_{68}$ cluster in all isomers. The motifs of initial and optimized structures for three isomers are presented in Fig. 3. The calculated relative averaged atomic binding energies (ΔE_b) for each isomer, with respect to cage-like $\text{Ti}_{12}\text{C}_{68}$ cluster, is written underneath each isomer.

Then, we evaluated the dynamical stability of the cage-like $\text{Ti}_{12}\text{C}_{68}$ by calculating the vibrational frequencies. Here, the harmonic vibrational frequencies are computed by diagonalizing the mass-weighted second-derivative matrix. There is no imaginary frequencies, which further validates the stability of cage-like $\text{Ti}_{12}\text{C}_{68}$ configuration. The lowest vibrational frequency and highest vibrational frequency corresponds to 95.1 cm^{-1} and 1423.9 cm^{-1} , respectively. To provide more information for future experimental identification, we simulated Raman spectrum, which is based on the Raman effect of inelastic scattering of monochromatic light. The energy shift is defined by the vibrational frequency and the proportion of the inelastically scattered light is defined by the spatial derivatives of the macroscopic polarization, technical details are described by Porezag and Pederson⁴². A Raman spectra with the temperature of 300 K and incident light of 488.0 nm was displayed in Fig. 4. We can see clearly that the spectrum has strong peaks at 98.7 and 273.1 cm^{-1} which are due to the Ti-C and C-C stretching modes respectively. More detailed data are described in the Supporting Information (Section I). Therefore, the cage-like $\text{Ti}_{12}\text{C}_{68}$ cluster is kinetically stable.

In what follows, we try to confirm the thermal stability of cage-like $\text{Ti}_{12}\text{C}_{68}$ cluster from *ab initio* NVE MD simulations with the initial temperature at 1400 K, 1800 K, 2000 K, 2200 K and 2400 K, which correspond the

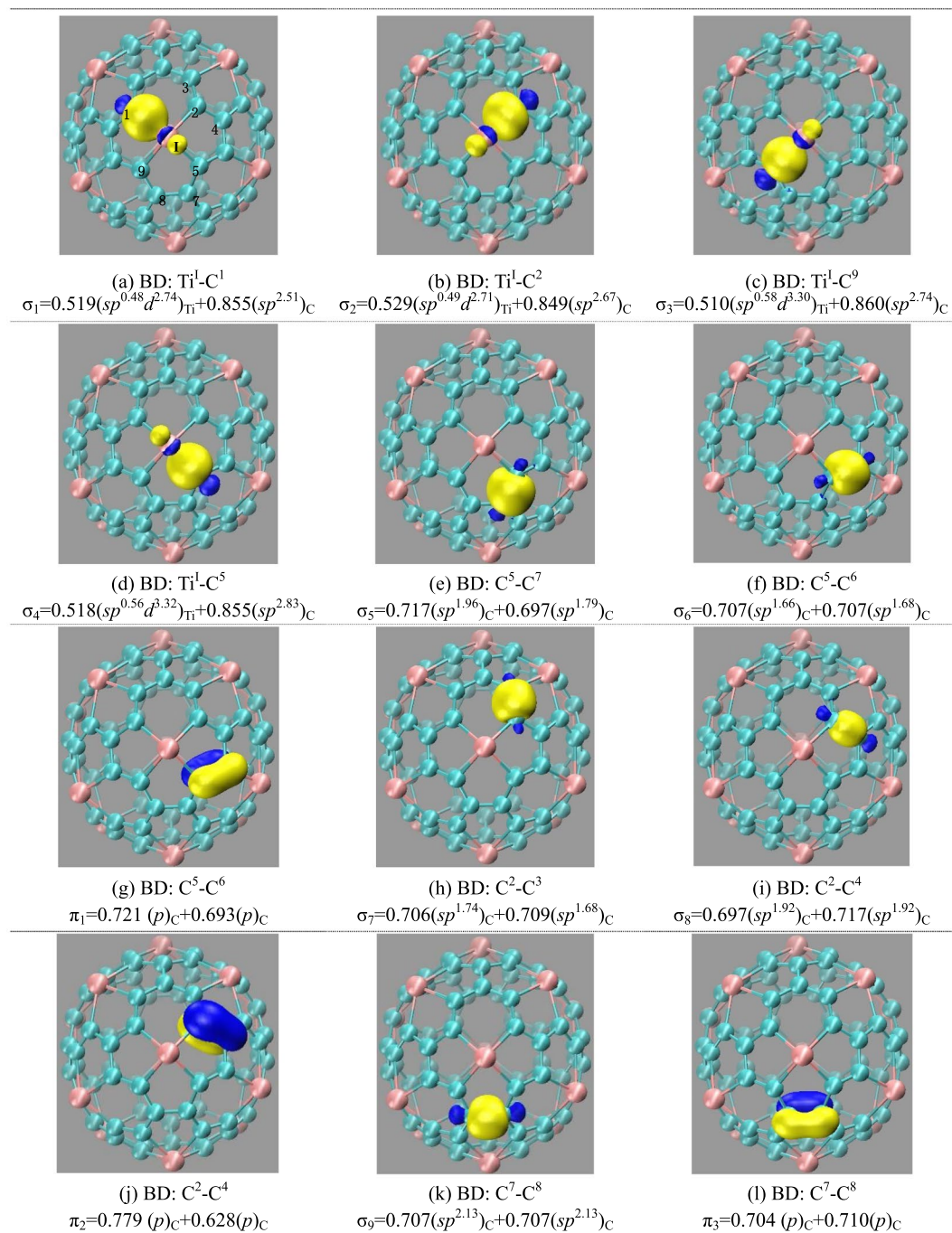


Figure 6. Some typical natural bond orbitals of $\text{Ti}_{12}\text{C}_{68}$ cage. BD is short for 2c-2e bond, and under each structure the detailed hybridization types are provided. All the configurations are viewed by the same orientations.

effective temperatures of 678 K, 877 K, 950 K, 1072 K and 1139 K. More detail information is presented in the Figs. S1 and S2, where the configurations snapshots of cage-like $\text{Ti}_{12}\text{C}_{68}$ cluster are shown at the 1.25 ps, 2.5 ps, 3.75 ps and 5 ps of each MD simulation. After 5 ps simulation, the topological structure of cage-like $\text{Ti}_{12}\text{C}_{68}$ cluster was well maintained when the initial temperature is up to 2400 K with the effective temperature of 1139 K. The above observation is an indication of high thermal stability for the cage-like $\text{Ti}_{12}\text{C}_{68}$ cluster.

To get insight into bonding properties of cage-like $\text{Ti}_{12}\text{C}_{68}$ cluster, Fig. 5c displays the deformation electron density, which reveals that electrons are donated from Ti to the C atoms. The removed electrons are mainly from the Ti 3d state, and are mainly delocalized to surrounding the four Ti-C bonds. For the Ti atoms, each Ti can connect with four carbon atoms through Ti-C σ bonds. For the carbons that adjacent to Ti atom, each carbon forms σ bonds with neighboring two carbons. Meanwhile, the natural bond orbital (NBO) analysis further elucidates the detailed type of hybridization. Some typical NBO are presented in the Fig. 6. The occupation numbers of natural

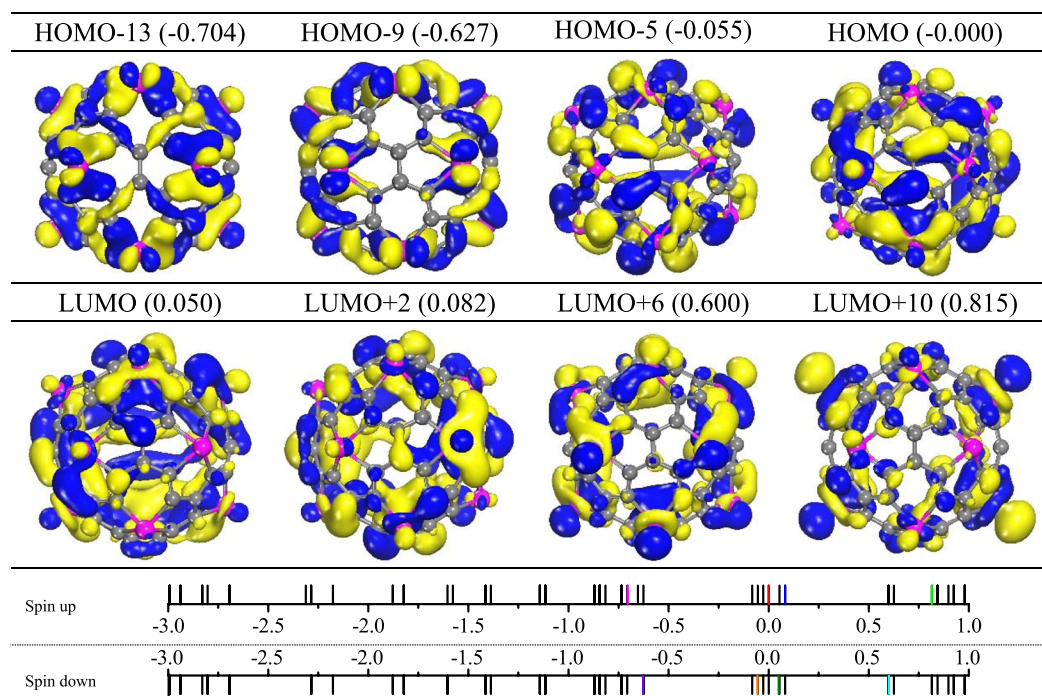


Figure 7. Frontier molecular orbitals for $\text{Ti}_{12}\text{C}_{68}$ cage. The locations of the above molecular orbitals are marked by different color lines, i.e. HOMO: red, HOMO–13: magenta, LUMO + 2: blue, LUMO + 10: green, LUMO: olive, HOMO–5: orange, HOMO–9: violet and LUMO + 6: cyan. The isovalues are $0.015 e/\text{\AA}^3$. The eigenvalues are given in brackets with the unit of eV.

orbitals are in the range from 1.59 to 1.97 electrons. Here, we label one Ti atom by roman numerals I, C atoms by arabic numerals 1, 2, 3, 4, 5, 6, 7, 8 and 9 as shown in Fig. 6(a). For the Ti^1 atom, four lobes of d orbit form four σ bonds with the neighboring four carbons (C^1 , C^2 , C^5 and C^9) atoms, as plotted Fig. 6(a–d). In the $\sigma_4(\text{Ti}^1\text{-C}^5)$ bond, it is a two-center two-electron ($2c\text{-}2e$) σ bond with the occupation numbers of 1.87 electrons in hexagon, in which the 26.85% and 73.15% of occupation numbers are situated on the Ti^1 atom and C^5 atom, respectively. The bond orbital of the Ti^1 atom mainly comes from the d orbital, and for the C^5 atom, the hybrids of $sp^{2.83}$ are a distorted sp^3 hybridization. In addition, C^5 atom form two σ (σ_5 and σ_6) bonds and a π_1 bond with two neighbor carbons shown in the Fig. 6(e–g), demonstrating the distortion sp^2 hybridization character of C^5 atom. For the $\sigma_2(\text{Ti}^1\text{-C}^2)$ bond comes from the hybridization of $sp^{0.49}d^{2.71}$ on Ti^1 atom and $sp^{2.67}$ on the C^2 carbon in the hexagon as plotted in Fig. 6(b). It is noted that C^2 atom link the neighbor C^3 atom and C^4 atom by σ bonds plotted in Fig. 6(h) and (i), and a π_2 bond which is formed by the hybridization between p orbital of C^2 atom and p orbital of C^4 atom, as shown in Fig. 6(j). In addition, two identical pentagons are connected by the $\text{C}^7\text{-C}^8$ bond, from the Fig. 6(k) and (l), it can be seen that C^7 atom form σ bond and π_2 bond with the neighboring C^8 atom. For the all $\sigma(\text{C-C})$ bonds, it can be found that major contribution comes from sp^2 -like hybridization of C atom.

Finally, to investigate the electronic structures of cage-like $\text{Ti}_{12}\text{C}_{68}$ cluster. We plotted the projected density of states (PDOS) in Fig. 5a. As can be seen from Fig. 5a, the HOMO and LUMO orbitals show strong $p\text{-}d$ hybridization. The region of 0.6 eV to 1.0 eV and below -0.6 eV, there is $sp\text{-}d$ hybridization character. Furthermore, the plots of frontier orbitals, including HOMO, HOMO–5, HOMO–9, HOMO–13, LUMO, LUMO + 2, LUMO + 6, and LUMO + 10 are given in Fig. 7. As seen from Fig. 7, π bonds form between carbons (for example, HOMO and HOMO–5), which is crucial for stabilizing the structures of cage-like $\text{Ti}_{12}\text{C}_{68}$ cluster. For the HOMO, LUMO, LUMO + 2, LUMO + 6, and LUMO + 10 orbitals, the d_{z^2} -like orbitals and other d_{xy} -like (d_{xy} , d_{yz} , d_{xz}) orbitals characteristic appear on the Ti atoms. Especially for LUMO + 6, and LUMO + 10, orbitals characteristic mainly focus on the Ti atoms. However, HOMO-5, HOMO-9 and HOMO-13 orbitals display sole d_{xy} -like orbital characteristics on the Ti atoms. While all the given frontier orbitals on C atoms mainly exhibit the p orbital character. The above observations are in concordance with the natural bond orbital analysis.

Conclusions

In summary, we have discovered a stable cage-like $\text{Ti}_{12}\text{C}_{68}$ cluster with T_h symmetry. The stability of cage-like $\text{Ti}_{12}\text{C}_{68}$ cluster has been confirmed using the molecular dynamics simulations and the vibrational frequency analysis. Meanwhile, this cluster is found to have a relatively small HOMO-LUMO gap, which suggests strong chemical activity. More importantly, the density of states and frontier orbitals distributions show remarkable orbital hybridization. The natural bond orbital analysis provides a detailed description including the bond-type of hybridization and occupancy numbers, results show that four lobes of d orbit for each Ti atom form four σ bonds with the neighboring four carbons atoms in each TiC_{13} subunit playing a significant role in the structural stability. Moreover, the calculated Raman spectrum of cage-like $\text{Ti}_{12}\text{C}_{68}$ should provide more information for

future experimental observations and synthesis. If this molecule can be prepared in a future experiment, it would enrich the species of hollow metal carbide clusters or analogues of metallo-carbohedrenes.

Computational details

All theoretical calculations are on the basis of the density functional theory (DFT), which begins with a theorem by Hohenberg and Kohn⁴³, later generalized by Levy⁴⁴, and in which all ground-state properties are functionals of the charge density. For the considered system, except kinetic energy and the classical electrostatic energy, it includes all many-body contributions to the total energy, in particular, the exchange and correlation energies. The exchange-correlation energy, requires some approximation for this method to be computationally tractable. A popular and good approximation is the gradient-corrected approximation (GGA), which can provide a considerable increase in the accuracy of predicted energies and structures as to the local density approximation (LDA). In our calculations, three different exchange-correlation functionals, the Perdew-Burke-Ernzerhof correlation (PBE)⁴⁵, Perdew-Wang (PW91)⁴⁶, and Becke exchange plus Lee-Yang-Parr correlation (BLYP)^{47,48}, were employed. For the basis functions, the double numerical including polarization (DNP)⁴⁹ were utilized with the best accuracy and highest cost. For C atom, it is $1s2s2p2s'2p'3d$, and it is $1s2s2p3s3p3d4s3d'4s'4p$ for Ti atom. All geometry optimizations of cage-like $Ti_{12}C_{68}$ clusters were performed using spin-unrestricted and symmetry-unconstrained.

Ab initio molecular dynamics (MD) simulations, the most natural method of performing equilibrium statistical-mechanical calculations, was selected to evaluate the thermal stability of $Ti_{12}C_{68}$ cage. The constant energy, constant volume ensemble (NVE), also known as the microcanonical ensemble, was used. In the NVE ensemble, the total time was set to be 5 ps, with each step taking 1.0 fs at initial temperature of 1400 K, 1800 K, 2000 K, 2200 K and 2400 K. The natural bond orbital (NBO), that describe the Lewis-like molecular bonding pattern of electron pairs in optimally compact form, is analyzed at the LANL2DZ basis set in Gaussian 09 package⁵⁰.

References

- Wang, J., Ma, H. M. & Liu, Y. $Sc_{20}C_{60}$: a Volleyballene. *Nanoscale* **8**, 11441–11444 (2016).
- Wang, J. & Liu, Y. New Volleyballenes: $Y_{20}C_{60}$ and $La_{20}C_{60}$. *Sci. Rep.* **6**, 30875–1–5 (2016).
- Guo, B. C., Wei, S., Purnell, J., Buzza, S. & Castleman, A. W. Jr. Metallo-Carbohedrenes [$M_8C_{12}^+$ ($M = V, Zr, Hf$, and Ti)]: A Class of Stable Molecular Cluster Ions. *Science* **256**, 515–516 (1992).
- Wei, S., Guo, B. C., Purnell, J., Buzza, S. & Castleman, A. W. Jr. Metallo-carbohedrenes as a Class of Stable Neutral Clusters: Formation Mechanism of M_8C_{12} ($M = Ti$ and V). *J. Phys. Chem.* **96**, 4166–4168 (1992).
- Pilgrim, J. S. & Duncan, M. A. Metallo-Carbohedrenes: Chromium, Iron, and Molybdenum Analogues. *J. Am. Chem. Soc.* **115**, 6958–6961 (1993).
- Dance, I. Geometric and Electronic Structures of [Ti_8C_{12}]: Analogies with C_{60} . *J. Chem. Soc., Chem. Commun.* **24**, 1779–1780 (1992).
- Dance, I. Ti_8C_{12} : Barrierless Transformation of the T_h Isomer to the T_d Isomer. *J. Am. Chem. Soc.* **118**, 6309–6310 (1996).
- Lin, Z. & Hall, M. B. Theoretical studies on the stability of M_8C_{12} clusters. *J. Am. Chem. Soc.* **115**, 11165–11168 (1993).
- Rohmer, M. M., Bénard, M., Bo, C. & Poblet, J. Ab Initio SCF and CI Investigations on Titanium-Carbon Clusters: Metallo-carbohedrenes Ti_8C_{12} and Cfc Crystallites $Ti_{14}C_{13}$. *J. Am. Chem. Soc.* **117**, 508–517 (1995).
- Bénard, M., Rohmer, M. M., Poblet, J. & Bo, C. Diversity in the Electronic Structures of Metallo-carbohedrenes: Ab Initio Study of M_8C_{12} ($M = Ti, V, Zr, Nb$) and $Ti_4M'_4C_{12}$ ($M' = V, Zr$). *J. Phys. Chem.* **99**, 16913–16924 (1995).
- Chen, H., Feyereisen, M., Long, X. P. & Fitzgerald, G. Stability, bonding, and geometric structure of Ti_8C_{12} , Ti_8N_{12} , V_8C_{12} , and Zr_8C_{12} . *Phys. Rev. Lett.* **71**, 1732–1735 (1993).
- Gueorguiev, G. K. & Pacheco, J. M. Structural Identification of Metcars. *Phys. Rev. Lett.* **88**, 115504 (2002).
- Baruah, T., Perderson, M. R., Lyn, M. L. & Castleman, A. W. Jr. Predicted infrared and Raman spectra for neutral Ti_8C_{12} isomers. *Phys. Rev. A* **66**, 053201 (2002).
- Deng, K., Duan, W. & Gu, B. Theoretical studies on the electronic structure of Ti_8C_{12} isomers. *J. Chem. Phys.* **121**, 4123–4126 (2004).
- Sohby, M. A., Castleman, A. W. Jr. & Sofo, J. O. A density-functional study of the structural, electronic, magnetic, and vibrational properties of Ti_8C_{12} metallo-carbohedrynes. *J. Chem. Phys.* **123**, 154106 (2005).
- Martinez, J. I., Castro, A., Rubio, A. & Alonso, J. A. Photoabsorption spectra of Ti_8C_{12} metallo-carbohedrynes: Theoretical spectroscopy within time-dependent density functional theory. *J. Chem. Phys.* **125**, 074311 (2006).
- Harris, H. & Dance, I. The Geometric and Electronic Structures of Niobium Carbon Clusters. *J. Phys. Chem. A* **105**, 3340–3358 (2001).
- Hou, H., Muckerman, J. T., Liu, P. & Rodriguez, J. A. Computational Study of the Geometry and Properties of the Metcars Ti_8C_{12} and Mo_8C_{12} . *J. Phys. Chem. A* **107**, 9344–9356 (2003).
- Wang, L. S. & Cheng, H. S. Growth Pathways of Metallo-carbohedrenes: Cagelike or Cubic? *Phys. Rev. Lett.* **78**, 2983–2986 (1997).
- Wang, L. S., Wang, X. B., Wu, H. & Cheng, H. New Magic Numbers in $Ti_4C_y^-$ Anion Clusters and Implications for the Growth Mechanisms of Titanium Carbide Clusters. *J. Am. Chem. Soc.* **120**, 6556–6562 (1998).
- Ganji, M. D., Sohbatazadeh, Z. & Khosravi, A. Spin-dependent transport characteristics of Fe met-cars. *Struct. Chem.* **25**, 551–559 (2014).
- Clayborne, P. A., Jones, C. E. Jr., Gupta, U., Melko, J. J., Khanna, S. N. & Castleman, A. W. Jr. Structural Evolution of Triniobium Carbide Clusters: Evidence of Large C_n Chains ($n = 3–4$) in $Nb_3C_n^-$ ($n = 5–10$) Clusters. *J. Phys. Chem. A* **114**, 1290–1297 (2010).
- Joswig, J. O., Springborg, M. & Seifert, G. Structural and electronic properties of small titanium-carbon clusters (metcars). *Phys. Chem. Chem. Phys.* **3**, 5130–5134 (2001).
- Fukushima, N., Miyajima, K. & Mafune, F. Ionization Energies of Niobium Carbide Clusters Nb_nC_m ($n = 3–10, m = 0–7$). *J. Phys. Chem. A* **113**, 2309–2315 (2009).
- Van Heijnsbergen, D., Von Helden, G., Duncan, M. A., van Rooij, A. J. A. & Meijer, G. Vibrational Spectroscopy of Gas-Phase Metal-Carbide Clusters and Nanocrystals. *Phys. Rev. Lett.* **83**, 4983–4986 (1999).
- Dryza, V., Alvino, J. F. & Metha, G. F. Onset of Carbon-Carbon Bonding in Ta_3C_y ($y = 0–6$) Clusters: A Threshold Photoionization and Density Functional Theory Study. *J. Phys. Chem. A* **114**, 4080–4085 (2010).
- Chernyy, V., Logemann, R., Bakker, J. M. & Kirilyuk, A. Determination of the geometric structure of neutral niobium carbide clusters via infrared spectroscopy. *J. Chem. Phys.* **145**, 164305 (2016).
- Cruz-Olvera, D. & Calaminici, P. Investigation of structures and energy properties of molybdenum carbide clusters: Insight from theory. *Comput. Theor. Chem.* **1078**, 55–64 (2016).
- Akman, N., Durgun, E., Yildirim, T. & Ciraci, S. Hydrogen storage capacity of titanium met-cars. *J. Phys.: Condens. Matter* **18**, 9509–9517 (2006).

30. Liu, P. *et al.* Gas-phase Interaction of Thiophene with the $\text{Ti}_8\text{C}_{12}^+$ and Ti_8C_{12} Met-Car Clusters. *J. Phys. Chem. B* **110**, 7449–7455 (2006).
31. Bora, P. L. & Singh, A. K. New insights into designing metallocarborane based room temperature hydrogen storage media. *J. Chem. Phys.* **139**, 164319 (2013).
32. Chaur, M. N., Melin, F., Ortiz, A. L. & Echegoyen, L. Chemical, Electrochemical, and Structural Properties of Endohedral Metallofullerenes. *Angew. Chem. Int. Ed.* **48**, 7514–7538 (2009).
33. Yamada, M., Mizorogi, N., Tsuchiya, T., Akasaka, T. & Nagase, S. Synthesis and Characterization of the D_{5h} Isomer of the Endohedral Dimetallofullerene $\text{Ce}_2@C_{80}$: Two-Dimensional Circulation of Encapsulated Metal Atoms Inside a Fullerene Cage. *Chem. Eur. J.* **15**, 9486–9493 (2009).
34. Yang, T., Zhao, X. & Nagase, S. Di-lanthanide encapsulated into large fullerene C_{100} : a DFT survey. *Phys. Chem. Chem. Phys.* **13**, 5034–5037 (2011).
35. Heath, J. R. *et al.* Lanthanum complexes of spheroidal carbon shells. *J. Am. Chem. Soc.* **107**, 7779–7780 (1985).
36. Akasaka, T. *et al.* ^{13}C and ^{139}La NMR Studies of $\text{La}_2@C_{80}$: First Evidence for Circular Motion of Metal Atoms in Endohedral Dimetallofullerenes. *Angew. Chem. Int. Ed. Engl.* **36**, 1643–1645 (1997).
37. Wang, C. R. *et al.* A Scandium Carbide Endohedral Metallofullerene: $(\text{Sc}_2\text{C}_2)@C_{84}$. *Angew. Chem. Int. Ed.* **40**, 397–399 (2001).
38. Cai, W., Li, F. F., Bao, L., Xie, Y. & Lu, X. Isolation and Crystallographic Characterization of $\text{La}_2\text{C}_2@C_3(574)-C_{102}$ and $\text{La}_2\text{C}_2@C_2(816)-C_{104}$: Evidence for the Top-Down Formation Mechanism of Fullerenes. *J. Am. Chem. Soc.* **138**, 6670–6675 (2016).
39. Zhang, J. *et al.* Nanoscale Fullerene Compression of an Yttrium Carbide Cluster. *J. Am. Chem. Soc.* **134**, 8487–8493 (2012).
40. Yang, S., Wei, T. & Jin, F. When metal clusters meet carbon cages: endohedral clusterfullerenes. *Chem. Soc. Rev.* **46**, 5005–5058 (2017).
41. Kato, H. *et al.* Lanthanoid Endohedral Metallofullerenols for MRI Contrast Agents. *J. Am. Chem. Soc.* **125**, 4391–4397 (2003).
42. Porezag, D. & Pederson, M. R. Infrared intensities and Raman-scattering activities within density-functional theory. *Phys. Rev. B* **54**, 7830–7836 (1996).
43. Hohenberg, P. & Kohn, W. Inhomogeneous electron gas. *Phys. Rev.* **136**, B864–871 (1964).
44. Levy, M. Universal variational functionals of electron densities, first-order density matrices, and natural spin-orbitals and solution of the v -representability problem. *Proc. Natl. Acad. Sci. USA* **76**, 6062–6065 (1979).
45. Perdew, J. P., Burke, K. & Ernzerhof, M. Generalized Gradient Approximation Made Simple. *Phys. Rev. Lett.* **77**, 3865–3868 (1996).
46. Perdew, J. P. & Wang, Y. Accurate and simple analytic representation of the electron-gas correlation energy. *Phys. Rev. B* **45**, 13244–13249 (1992).
47. Lee, C., Yang, W. & Parr, R. G. Development of the Colle-Salvetti correlation-energy formula into a functional of the electron density. *Phys. Rev. B* **37**, 785–789 (1988).
48. Becke, A. D. Density-functional exchange-energy approximation with correct asymptotic behavior. *Phys. Rev. A* **38**, 3098–3100 (1988).
49. Delley, B. J. An all-electron numerical method for solving the local density functional for polyatomic molecules. *Chem. Phys.* **92**, 508–517 (1990).
50. Frisch, M. J. *et al.* Gaussian 09 Revision C.01; (Gaussian, Inc., Wallingford, CT, 2010).

Acknowledgements

This work is supported by the National Natural Science Foundation of China (Grant Nos. 11274089, U1331116, 11304076, and 11547198), the Natural Science Foundation of Hebei Province for Distinguished Young Scholar (Grant No. A2018205174), and the Program for High-level Talents of Hebei Province (Grant No. A201500118). We also acknowledge partially financial support from the 973 Project in China under Grant No. 2011CB606401.

Author Contributions

Y. Liu conceived the calculation methods and the research contents, L.Y. Ai conducted the calculations, L.Y. Ai, H.Y. Zhao and Y. Liu analysed the results. All authors reviewed the manuscript.

Additional Information

Supplementary information accompanies this paper at <https://doi.org/10.1038/s41598-018-22381-y>.

Competing Interests: The authors declare no competing interests.

Publisher's note: Springer Nature remains neutral with regard to jurisdictional claims in published maps and institutional affiliations.



Open Access This article is licensed under a Creative Commons Attribution 4.0 International License, which permits use, sharing, adaptation, distribution and reproduction in any medium or format, as long as you give appropriate credit to the original author(s) and the source, provide a link to the Creative Commons license, and indicate if changes were made. The images or other third party material in this article are included in the article's Creative Commons license, unless indicated otherwise in a credit line to the material. If material is not included in the article's Creative Commons license and your intended use is not permitted by statutory regulation or exceeds the permitted use, you will need to obtain permission directly from the copyright holder. To view a copy of this license, visit <http://creativecommons.org/licenses/by/4.0/>.

© The Author(s) 2018